ARTICLE TYPE

Formation of wafer-scale monolayer close-packed colloidal crystal of polystyrene spheres via thermally assisted self-assembly

X.Y.Z[a]

We developed a versatile, reliable, nonlithographic approach to create wafer-scale monolayer hexagonal close-packed polystyrene (PS) spheres arrays, namely colloidal crystal, which is greatly potential in various applications. The method combines spin-coating and thermal treatment, and the latter plays a key role to form high-quality colloidal crystal. We introduced a new dispersion system consisting of glycol
10 and ethanol to assist the thermal treatment. Moreover, based on the new process, we improved the traditional self-assembly theory and then simulated the thermally assisted self-assembly process with a modified Monte Carlo method. Consequently, we are able to understand the procedure better and predict the optimized self-assembly temperature as well. To our best knowledge, we report the method, namely achieving colloidal crystal using thermally assisted self-assembly and computer simulation, for the first
15 time. In addition, we indicate that this method could also be used to assemble PS spheres with other diameters and other kinds of spheres.

1. Introduction

There has been enormously widespread interest in colloidal crystal for several decades because of its potential applications in
20 nano-lithography,[1-3] photonics,[4-6] data storage,[7, 8] biosensors,[9] and plasmonics.[10-12] A rich variety of methods have been developed for the crystallization. All the techniques can be divided into two categories:[13] direct assembly on a solid substrate[14] and liquid interface-mediated processes.[15] Although the interface-mediated
25 processes possess the inherent benefits of less restriction of substrates and nature of formation of monolayers, it is not applicable to some special substrates or devices. In the contrary, the direct assembly methods are not only experimentally more straightforward as they do not require any special instruments,
30 but also of higher flexibility in the preparation of different colloid arrangements with pre-structured substrates. The direct assembly methods can be further divided into two subcategories:[13] evaporation induced processes and processes using external forces. The evaporation induced methods can obtain monolayers
35 with a high degree of crystallinity if experimental conditions (including ambient temperature and humidity) are tightly controlled. However, they are inherently rather slow and sensitive to the meniscus of solvent front, which may lead to ruptures in the resulting monolayer.[16] Moreover, there are great challenges
40 for evaporation induced methods that the very tight control over both experimental and ambient conditions which can be demanding to regulate and cumbersome to optimize. Another serious limition of the evaporation induced processes are only capable of generating colloidal crystals built up by small
45 domains, whose scaling-up to an industrial-scale mass-fabrication seems infeasible due to their tedious fabrication processes and

incompatibility to wafe-scale batch microfabrication widely used by the semiconductor industry.[17]
Very recently, Yunker and his co-workers have shown
50 experimentally that the shape of the suspended particles is important and can be used to eliminate the coffee-ring effect.[18] They found the particle shape provides a convenient parameter to the depositon of particles. However, it is not suitable for the shape of sphere-like, which is widely used in colloid self-
55 assembly. Khunsin et al found assembling colloidal crystals in a moving menicus under random noise agitation would produce better opal film.[19] Spin-coating method[20-22] is an alternative strategy to overcome the drawbacks mentioned above. However, there are few reports using this method to prepare polystyrene
60 spheres monolayer crystal. Fischer et al[22] directly spread a droplet of latex spheres on the glass and harvested 10 μm in length monolayer spheres. The obtained crystal had imperfections including point defects, dislocations, and grain boundaries. Subsequently, Deckman's group[20] developed spin coating to
65 define a low ordered spheres polycrystal, of which area was still much smaller than an industrial wafer size. And the use of surfactants was an essential step, which in turn may reduce the capabilities of the produced nano-materials for the presence of surfactant impurities.
70 Here we show a micro- or nano-fabrication technique, combining spin coating and thermal treatment, which textures wafer-scale surface areas with monolayer hexagonal close-packed PS spheres. The procedure will be described in greater detail in the experimental section. Briefly, suspension liquid composed of
75 colloidal spheres with the desired diameter is deposited on a silicon surface by spin coating and the sample is subsequently sent into a oven for thermal treatment. Through a mass of

repeated experiments, we found that a wafer-scale and high ordered monolayer crystal with few defects could be achieved using thermal treatment. Additionally, we do not need surfactant in solution, nor do we need electrically charge the particles. And there is also no confinement between any boundaries or surface pressure control. It is considerable that our procedure is compatible with the semiconductor industry. Moreover, we improved the theory of PS spheres self-assembly based on thermal treatment and then simulated the self-assembly process with the modified Monte Carlo method, which is able to predict the optimized self-assembly temperature. With the simulation, we only need few experiments to achieve the best quality colloidal crystals. It is worth to mention here that the simulation of crystallization is a really challenge work and few publications are in literatures to date. Skjeltorp's group presented an experimental study of crack growth in a two-dimensional system, using a monolayer of uniformly sized microspheres confined between two parallel sheets of glass and simulated the fracture in microsphere monolayers.[23] And they were indifferent from the process of aggregation behavior of PS spheres. Additionally, it is impossible to describe the dynamics of self-assembly process involving Brownian Motion for such a many-bodys system. We dealt with the troublesome problem by energy approach and introduced the potential energy of cappilary forces[24], which predominates over the self-assembly process. We can predict the optimized self-assembly temperature and avoid the cumbersome process to optimise the self-assembly temperature. To our best knowledge, it is the first report on thermal treatment assisted colloidal crystal self-assembly with the help of computer simulation. We believe the study of the simple model systems can also provide insights into the more complex systems which are often of considerable practical importance.

2. Experimental section

2.1 Chemicals and Materials

The chemical reagents, such as styrene (≥99.0wt%), sodium hydroxide (≥96.0wt%), sodium dodecyl sulfate (CP grade), potassium peroxydisulfate (≥99.5wt%), ethylene glycol (≥99.0wt%) and ethanol (≥99.5wt%) were used as received without further purification, which were purchased from Sinopharm Chemical Reagent Co., Ltd. (SCRC). The resistivity of the deionized water (DI water) is 18.25 (MΩ·cm). Silicon wafer with the size of 1.5cm×1.5cm and another four-inch wafer were cleaned according to the RCA procedure[25] and subsequently cleaned in Piranha solution (70%H_2SO_4+30%H_2O_2) for 12h, followed by triple rinsing in DI water.

2.2 Structure Observation and Classification

The structure and Morphology of the resultant colloidal crystal were examined by field emission scanning electron microscopy (SEM, JSM-6700F) operating at 5KV. The corresponding Fourier Transform (FT) patterns were obtained by the two-dimensional Discrete Fourier Transform (DFT) technique:

$$F(u,v) = \sum_{x=0}^{M-1} \sum_{y=0}^{N-1} f(x,y) \exp\left(-i2\pi ux/M\right) \exp\left(-i2\pi vy/N\right) \quad (1)$$

where f(x, y) represents the spatial domain function and F(u, v) is the corresponding FT.

2.3 Synthesis of Monodisperse Polystyrene Spheres

Spherical polystyrene particles were synthesized by emulsion polymerizing of styrene in ethanol solution.[26] Briefly, 0.0538 g SDS and 0.0489 g KPS were dissolved in 70ml aqueous alcohol (ethanol-water volume ratio was 5:2) in a 250 ml three-neck flask. Then 2.2 ml styrene, which had been treated with 10% sodium hydroxide solution in a separatory funnel three times in order to remove the anti-polymerizer, was added under nitrogen atmosphere and rapid stirring, and the emulsion was heated to 70 ℃ to polymerize for 8 h.

2.4 Preparation of Colloidal Dispersions

The obtained polystyrene spheres were cleaned using successive centrifugation and ultrasonic cleaning in ethanol system three times. Prior to use, the purified polystyrene spheres were re-dispersed in different solvents, such as water, ethanol, miscible liquid of ethanol and glycol, and the final volume fraction was set to about 20%. Beside, for the dispersion of ethylene glycol and ethanol (using a 1:1 mixture of glycol/ethanol), the PS spheres latex with the volume fraction of 40% and 60% were also prepared.

2.5 Spin-coating of PS spheres Latex and thermal treatment

Certain volume of above colloidal latex was deposited on wafer substrate. The wafer was spin-coated at 550 rpm on a commercial spin coater (CAS, KW-4A) for 9 seconds to spread the PS latex and then the wafer was then quickly accelerated to 3500 rpm for 30 seconds. For some samples, Six-arm diffraction star were formed in about 15 seconds. After spin-coating, the substrates were transferred to an electric thermostatic drying oven with a quartz window for special time. The sample was dried from edge to center gradually and a variety of colors emerged in the end.
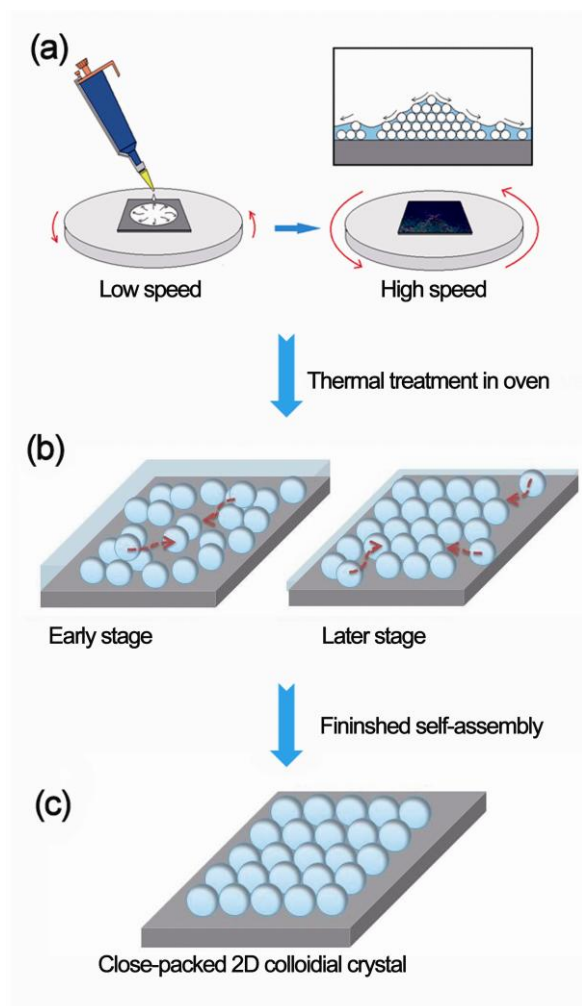
3. Results and discussion

A simple cartoon of the procedure to achieve monolayer layer hexagonal-close-packed PS spheres, namely monolayer colloidal crystal, is shown in Fig. 1. Certain volume of PS latex is deposited on a silicon wafer and the latex is spread all over the surface after spin-coating. Subsequently, the silicon wafer is then quickly transferred to an electric thermostatic drying oven for thermal treatment. When the latex film drys, monolayer colloidal crystal was forms.

3.1 The dispersion system for PS spheres

The diameter of the PS spheres we synthetized is (462 ± 20) nm (Figure S1). Large area close-packed spheres can be obtained only if the PS spheres latex spread uniformly onto the silicon surface. Thus, the latex must wet the silicon surface, which indicates the dispersion system for PS spheres is very important. We investigated different dispersion media, such as ethanol, water, a mixture solvents of ethanol and glycol. Except dispersion media, all other conditions, such as latex volume fraction (20%), spin coating time (30s), final spin coating speed (3500 rpm) and self-assembly temperature($45\,℃$) were the same.
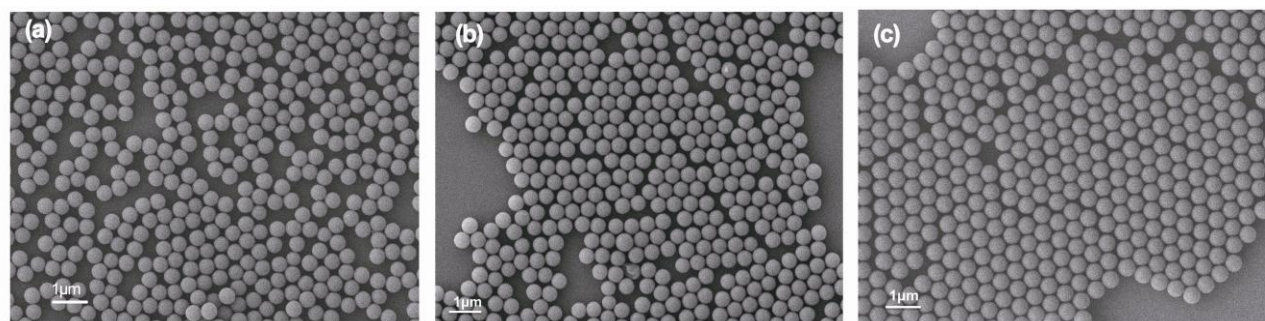

Fig. 2 Different dispersion media for PS spheres self-assembly: (a) ethanol; (b) water; (c) a mixture solvents of ethanol and glycol.

Although ethanol can wet the wafer, it drys before the spin-coating process is over. Time was too short to assemble the PS spheres. As shown in Fig. 2 (a), PS spheres arrays which used the dispersion system of ethanol, is an almost random arrays and it has a lot of small vacancies even polytrope. For the dispersion media of water, the quality of colloidal crystal has been greatly improved (Fig. 2 (b)), which is ascribe to the wetting time lasts longer than the ethanol's. However, it is still not enough for the self-assembly process because the liquid became dry in minutes at room temperature ($25\,℃$) after the spin-coating, which leaded to some line defects and small vacancies in Fig. 2 (b). There would be no chance to improve the quality of the colloidal crystal only if the self-assembly time can last long enough. The mixture liquid of ethanol and glycol dry in fifteen minutes when it is placed in 45 ℃ environment. Moreover, the mixture solvents liquid of ethanol and glycol can wet the spheres better and impose the stronger capillary force on PS spheres, which is key to making PS spheres close-packed. The crystal shown in Fig. 2 (c) using a mixture solvents of ethanol and glycol as dispersion media is packed more closely than others. The quality of colloidal crystal is sensitive to the self-assembly enviroment (such as temperature etc.) and the point defects can be found in Fig. 2 (c), namely a vacancy which can accommodate a PS sphere. The close-packed principle will be described in detail in section of "The mechanism of thermal treatment self-assembly". We used the mixture solvents of ethanol and glycol as dispersion media for

all the experiments in the sections below.

3.2 The thermal treatment assisted self-assembly colloidal crystal

In our previous experiments, we tried all kinds of latex concentration, but the obtained colloidal crystal was either not wafer-scale area covered or multilayer spheres in micro-region.
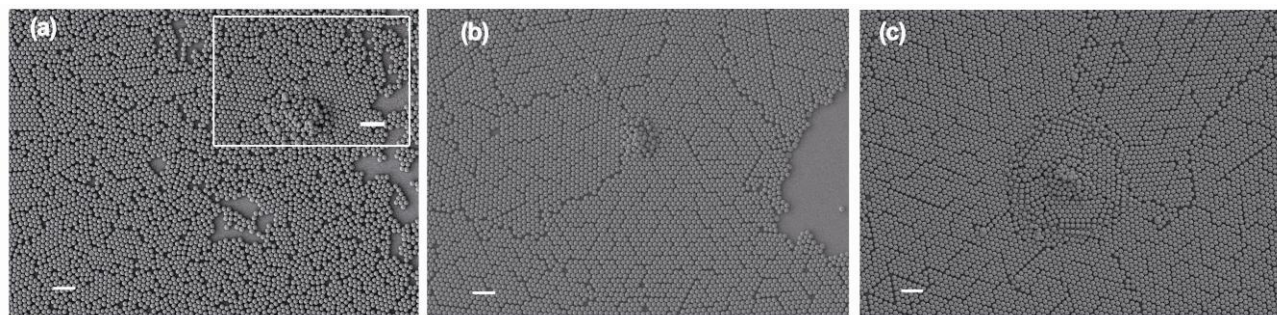
To overcome these drawbacks, we introduced thermal treatment and investigated temperature effects on the self-assembly. The typical results are shown in Fig. 3. Except self-assembly temperature, all other conditions, such as latex volume fraction (20%), spin coating time (30 s), and spin coating speed (3500rpm) were the same.

Fig. 3 Typical top-view SEM images of colloidal crystal by thermal treatment: (a) 35℃; (b) 65℃; (c) 85℃. Scale bar is 2 microns.

Fig. 3 (a) shows that the PS spheres are loose packing at the low temperature (35℃) because the capillary attraction is not strong enough. With increasing self-assembly temperature, the loose packing spheres gradually disappears and they would be close-packed when the temperature reaches to 65 ℃ (Fig. 3 (b)). But the degree of close packing of the PS spheres have not been improved when the temperature is further increased to 85 ℃ (Fig. 3 (c)). Another phenomenon shown in inset of Fig. 3 (a) is multilayer spheres emerging. It could be explained from Fig. 1. The latex was spread from the center of the silicon substrate to the edge during the spin-coating process, and the multilayer spheres are inevitable in some areas unless the latex concentration is extremely low. The multilayer spheres greatly decrease when the temperature increases (Fig. 3 (b)). However, multilayer spheres appears more seriously at the extreme high temperature, such as 85 ℃(Fig. 3 (c)). At the higher temperature, the liquid is evaporated more quickly and the capillary attraction became stronger, leading to more close-packed PS spheres. On the other hand, over-high temperature decreases the self-assembly time significantly, which leaves little chance to scatter the multilayer PS spheres into the monolayer PS spheres. Based on the above analysis, an optimum temperature parameter could be expected for the PS spheres self-assemlbly. However, it is a great challenge to identify the optimum temperature through repeated experiments. Herein, we develop a theory model and predict optimum temperature through computer simulation, which will be described in the section of "The mechanism of thermal treatment assisted self-assembly" and "Computer simulation of the self-assembly process with a modified Monte Carlo method". We found the optimum temperature is 45 ℃ for the 462 nm PS spheres self-assembly.

Khunsin and his co-workers have reported an interesting work,[27] namely noise-assisted crystallization of opal films. They found the crystal quality of opal films self-assembled from polymer spheres in a moving meniscus could be improved using the agitation by white noise acoustic vibrations. They explained the mechanism in terms of the stochastic resonance. In our work, the thermal treatment seems to acting the role of noise acoustic vibration to some extent. In the view of thermal dynamics and statistical physics, the PS spheres self-assembly is a process of crystal formation and thus a phase transition, moving towards the state with the minimum energy. The PS spheres would find the positions where they can form a state with minimum energy in the free energy landscape. For our samples consisting of hard PS spheres, the state with minimum free energy would be monolayer-hexagonal-close-packed. When the self-assembly process is under a lower temperature (such as room temperature), the Brownian motion is weak and thus the kinetic energy of a single PS spheres is low. Consequently, the ability of PS spheres to search ergodically for the free energy landscape was poor. When the temperature increases, the kinetic energy of the PS spheres increases correspondingly, leading to a greater movement range of the PS sphere, thus a promoted capability of the PS sphere to search for the state with the minimum energy. This is the role of the thermal treatment on the self-assembly to construct a better colloidal crystal.

3.3 Concentration adjustment for PS spheres self-assembly

As the spin-coating theory described by Middleman,[28] the final film thickness is in the form:

$$H \approx A / \omega\sqrt{t} \qquad (2)$$

where A is a constant determined by the viscosity and density of the solution, ω and t are the final speed and time of spin. The formula (2) reveals that final film thickness is inversely proportional to the final spin speed and the square root of the final spin time. To obtain the same thickness latex film, the higher rotation speed and longer rotation time are, the larger latex volume fraction is need. In this research, we set a proper rotation parameters, namely 3500 rpm for 30 seconds, to achieve the latex film. The obtained results are shown in Fig. 4.
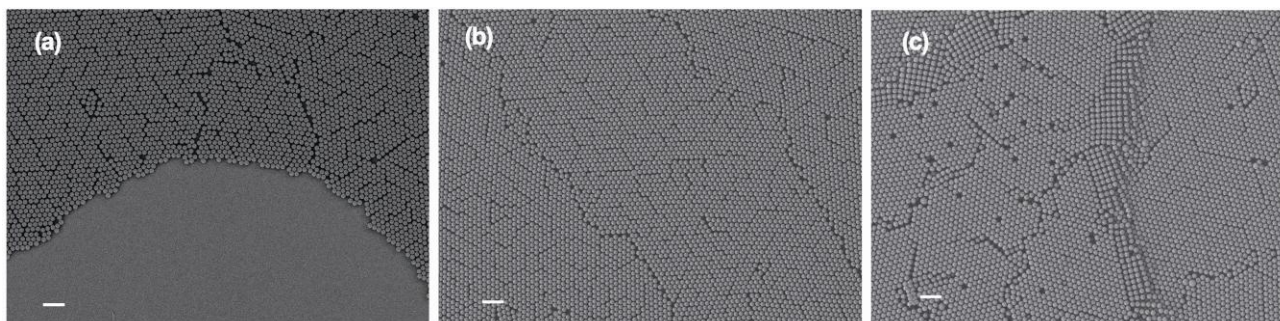
ARTICLE TYPE

Fig. 4 Different volume fractions (VF) for spin-coating: (a) 20%; (b) 40%; (c) 60%. Other conditions were the same: self-assembly temperature, final spin-coating speed and time were 45℃，3500 rpm and 30 seconds, respectively. Scale bar is 2 microns.

The areas covered by PS spheres becomes larger along with the
5 particle volume fraction rising. It is only about three fifths areas covered by PS spheres for the latex of VF=20% (Fig. 4 (a)). Wafer-scale monolayer close packed spheres forme for latex of VF=40% (Fig. 4 (b)). Multilayer spheres emerge seriously when the VF of the latex increased to 60%. An interesting feature is
10 evident that the cover area is not a simple linear function of latex VF.

We used the optimum condition, namely 40% particle volume fraction and 45 ℃ self-assembly temperature to achieve wafer-scale (*i.e.* four inch, *etc.*) monolayer-close-packed PS spheres
15 easily. To identify the features of monolayer and hexagonal close-packed, we randomly selected some areas to scan morphology using SEM, and the results are shown in Fig. 5.
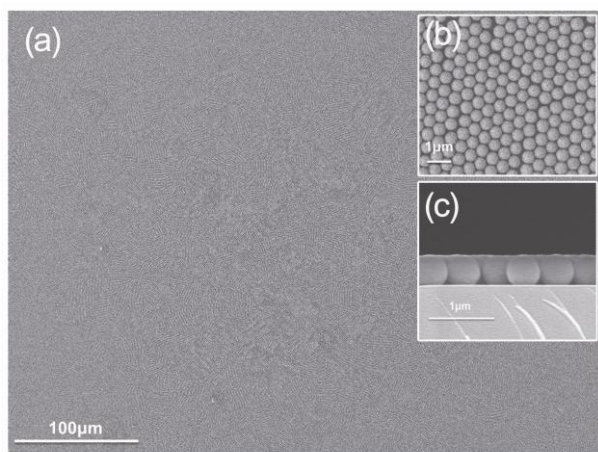

Fig. 5 SEM images of the colloidal crystal prepared by optimum
20 condition: (a) low magnification, top-view; (b) high magnification, top-view; (c) high magnification, side-view.

The hexagonal-close-packed cryatal is revealed from Figure 5 (b) and the monolayer is clearly revealed from the Figure 5 (c). More SEM images of monolayer colloidal crystal are available
25 seen in the supplementary information (Figure S2). The improved spin-coating technique described here has a number of

advantages over previous self-assembly. For example, it is rapid and highly manufacturable. A wafer-scale colloidal crystal, can be routinely made within half an hour, while early methods take
30 days or even weeks to produce a centimeter-size crystal.[29]

3.4 The mechanism of thermal treatment assisted self-assembly

In this section, we will develop the mechanism of PS spheres self-assembly based on Denkov's[14] and Kralchevsky's[30] work to
35 conform the thermal treatment process. The latex is spread uniformly onto the surface of the silicon substrate. However, as mentioned above, multilayers in some small domains are inevitable at room temperature. The thermal treatment can intensify the Brownian motion of the spheres in a mixture
40 solvents of ethanol and glycol, and the multilayers spheres are scattered into monolayer spheres (Fig. 6 (a)). Later, the slightly concave layer formed gradually owing to the liquid evaporation; when its thickness in the center of the area becomes equal to the particle's diameter, a nucleus of 2D crystal suddenly forms (Fig.
45 6 (b)). The liquid film around the particle deforms and capillary force arises. This deformation translates into a Laplace pressure that causes attraction of the identical colloids to minimize the curvature of the interface. The capillary forces are very long range and make the PS spheres close-packed. Surrounding liquid
50 level is higher than that of the center and convective force appears, governing PS spheres towards the ordered nucleus (Fig. 6 (c)). Point defects and line defects might appear if the spheres do not fit the space of two spheres' group well. Actually, the thermal treatment can enhance both the convective force and
55 capillary force because of the acceleration of the evaporating liquid, which makes the PS spheres pack closer and the self-assembly time become shorter.

We have shown the crucial role of the thermal treatment in the section of "The thermal treatment assisted self-assembly". It is a
60 great challenge to find the optimized temprature through experiments. Here we establish a model to predict the optimized self-assembly temperature. It is impossible to consider the detail dynamics of such huge amounts of PS spheres system. And we turned to the energy approach to analyse the crystallization

processes. The capillary force plays a leading role among all the forces imposing on the PS sphere (see supplementary information S3) and determines the quality of the resultant colloidal crystal. Thus it is reasonable to only consider the capillarity potential energy associated with the PS spheres system in the energy landscape. Kralchevsky and Nagayama have reported that the potential energy of the PS sphere reads[24]:

$$U_n = Q \ln \left(r_n \right) \qquad (3)$$

where the subscript n index the PS spheres to identify them and r_n is the distance beween the position of a certain particle and its corresponding nucleus. Q characterizes the ability of the particle to deform the liquid interface and the effect of the meniscus surface tension. For simplicity, we can write the Q as follows:

$$Q = U_0 = A e^{-\frac{\Delta}{k_B T}} e^{-\frac{s}{\tau_0 (1-\frac{T}{T_c})}} \qquad (4)$$

where A is a constant is τ_0 is "relaxation time" , T_c is the temperature of boiling point, k_B is the Boltzmann constant, s is the number of steps of Monte Carlo simulation, and $\triangle$ is the potential barrier of the PS sphere movement. U_0 consists of two terms ($\exp[-\Delta / k_B T]$ and $\exp[-s/\tau_0(1-T/T_c)]$) with clear physical interpretions. The former term of U_0 characterizes the effect of Brownian motion, which will promote the formation of monolayer PS spheres and find the minimum energy state in the free energy landscape. The latter one characterizes the evolutionary time under thermal treament, which will make the PS spheres more closer packed with the stronger capillary force.
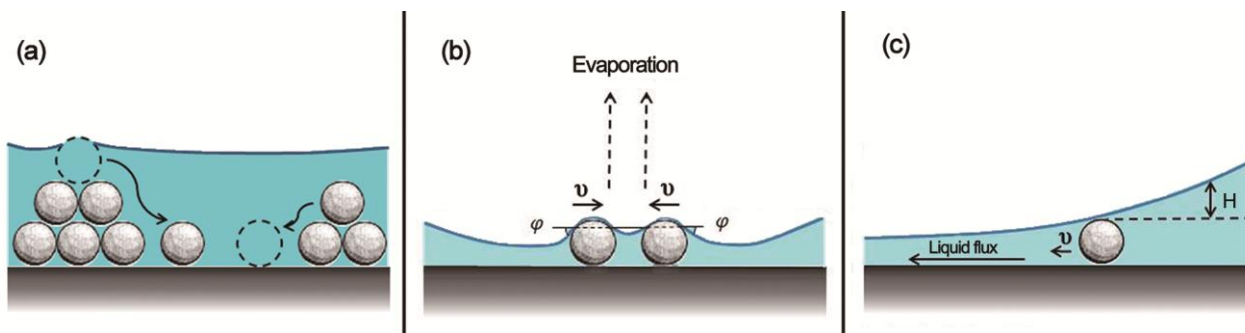

Fig. 6 The mechanism presentation of thermal treatment assisted self-assembly: (a) thermal treatment enhances the process of multilayer spheres breaking up into monolayer; (b) initial nucleation; (c) thermal treatment enhances spheres' transferring to nucleate areas.

3.5 Computer simulation of the self-assembly process with a modified Monte Carlo method

Here we will firstly introduce the assessment of ordering of spheres in the colloidal crystal and then discuss the Monte Carlo simulation of the self-assembly of PS spheres. We employ the well established method, namely two-dimensional Discrete Fourier Transform (DFT), to quantificationally evaluate the lattice ordering of the colloidal crystal.[19] For a perfect lattice, the sharp bright spots can be approximated by an arrays of delta functions, p(x), composed of m elements separated in space by an interval T,

$$p(x) = \sum_{m=-\infty}^{\infty} \delta(x - mT) \qquad (5)$$

The corresponding FT harmonics are all of the same magnitudes described by:

$$p(f) = \frac{1}{T} \sum_{n=-\infty}^{\infty} \delta(f - mf_0) \qquad (6)$$

where $f_0 = 1/T$. In contrast, the magnitude of a harmonic in a disordered lattice decreases with the harmonic index. Therefore, the ratio of the harmonic magnitudes quantifies the identity and the spatial resolution of the lattice points in the pattern. The uniformity of the lattice spacing across the image corresponds to the magnitude of the first harmonic. The apparently lower decrease rate of harmonic magnitudes points to a lower concentration of lattice defects.

The SEM images were captured with the same magnification, brightness, and contrast along the direction normal to the film. We carried out a statistical analysis on them. Each sample was examined base on a series of SEM images taken from 17 equidistant positions at 1mm separation across the sample. Fig. 7 illustrates the process of the quantitative assessment of the ordering of the colloidal crystal.
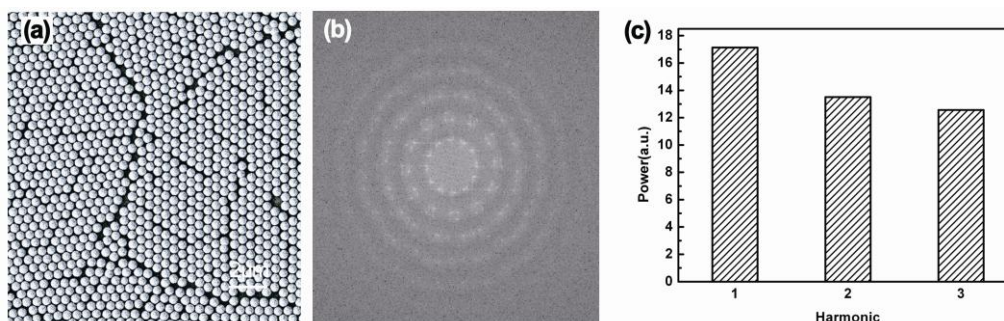
ARTICLE TYPE

Fig. 7 Process of the quantitative assessment the ordering of spheres in the growth plane: (a) typical scanning electron micrographs of colloidal crystal treated at the temperature of 35℃; (b) FT patterns of the SEM images in panel (a). The panel (c) shows the magnitude of the first three harmonics in the FT patterns shown in panel (b).

5 The colloidal crystal shown in Fig. 7 (a) is obtained under the condition of VF=20% and the self-assembly temperature, final spin-coating speed and time being 35℃, 3500 rpm and 30 seconds, respectively. Fig. 7 (b) shows the corresponding FT pattern. The bright spots are dim and not very regular, which 10 results from the loose packing and multilayer of arrays obtained at low temperature. In addition, diffuse rings appear due to azimuth misalignment of the lattices in colloidal crystal. The magnitudes of the first three harmonics (M1, M2, M3) in the FT pattern were shown in Fig. 7 (c) and they are 17.13, 13.51 and 15 12.56, respectively.

With the recent progress in the chemical synthesis and fabrication of colloidal particles and nanoparticles, there is unprecedented ability to control the interparticle interaction in such systems and the quality of colloidal crystal has been 20 improved. It is very clear that the optimiztion of the self-assembly parameters through experiments would suffer great challenge. Computer simulation is an alternative approach to overcome the challenge. Woodley and Catlow claim that "The predication of structure at the atomic lever is one of the most 25 fundamental challenges in condesed matter science".[31] And there are few reports on simulation of the spheres self-assembly. Wales and Scheraga[32] have applied Monte Carlo (MC) basin hopping algorithms to locate the minimum potential energy of the system, and as such, probe the zero-temperature phase behavior, which 30 breaks down for system when entropy plays a significant role. And Filion and his co-workers[33] presented an efficient and robust method based on MC simulation for predicting crystal structures at finite temperature and the method could be used in the condition where entropy plays a significant role. However, to the 35 best of our knowledge, there is no report on monolayer PS spheres self-assembly concerning the liquid evaporation. Here we present a new method based on MC simulation to predict the self-assembly temperature to achieve monolayer colloidal crystal.

The monolayer close-packed PS sphere arrarys is represented 40 by a triangular lattice (Figure S3). The side length of the lattice is equal to the diameter of the PS sphere. The whole region is divided into several nucleate areas and each area has one nucleus.

The nodes of the network are divied into two kinds, namely occupied and non-occupied, depending on whether the node has a 45 PS sphere or not. We assume that every particle only interacts with its nearest nucleus, so the potential energy of an occupied node, for example, the ith occupied node, is $U_i=U_0\ln(r_i)$, where r_i is the distance between any *ith* occupied node and its nearst nucleus. Thus the energy associated with this two-dimensional 50 network is given by:

$$U_{sum} = \sum_i U_i = \sum_i U_0 \ln\left(r_i\right) \qquad (7)$$

In additon, the morphology of the network keeps the same during the simulation process and each of the nodes is assumed to be bonded to an underlying rigid substrate by a realtively weak 55 bond, which could be neglected. Periodic boundary conditions are used in simulations so that every node is joined to six nearest neighbours.

At the start of each simulation, all the nodes are occupied with the same probability, which reflects different concentration of the 60 PS latex. The nodes can be divided into three different categories: (1) all neighbors are occupied, (2) some neighbors are occupied and (3) no neighbor is occupied. Some nodes were selected at random to be the nucleating points (denoted by *c* in Figure S3). As the simulation preceeds, we randomly select an occupied node 65 in category (2) to be the probe node(denoted by *s* in Figure S3). Since *s* falls into the latter two categories, the occupied probe particle could move into one of its un-occupied neighbors. The probability of particle above node *s* walking into the *jth* (1⩽j⩽ 6) un-occupied neighbors is given by

$$P_j \propto \exp[-(U_j - U_s)/k_BT] \qquad (8)$$

The normalized probability of the PS sphere moving from node *s* to node *k* reads

$$P_k^{'} = \frac{P_k}{\sum_j P_j} \qquad (9)$$

We generate a uniformly distributed random number $r \in [0, 1]$. If $0 < r < P_k^{'}$, we choose node k as the seleted particle's next potential position, while node k+1 is chosen if $P_k^{'} < r < P_{k+1}^{'}$, choose node $k+1$. A trial move to node n is accepted if the energy of the system decreases, i.e. $U_n < U_s$. Otherwise, the probability to accept this trial move is given by formula (8). In a word, probability for the probe particle to move from node s to node n is

$$P(n \rightarrow s) = \min[1, \; P_n] \qquad (10)$$

Each time when the PS sphere move is accepted, we update the corresponding change of energy of the system and prepare for the next Monte Carlo circulation and repeat above steps many times to simulate the self-assembly. We stop the simulation process when the fluctuation of the energy of the system δU_{sum} relative to the total change of energy of the system ΔU is smaller than the predefined final value [such as $\delta U_{sum}/\Delta U \leq 1\%$] (Figure S4).

We should point out here that the simulation of the PS spheres self-assembly is carried out in two dimensional (2D) plane and the simulation lattice was 100×100. Consequently, what we have taken into account in the simulation corresponds to the processes

illustrated in Fig. 6(b) and (c). However, our model still works because we had set the concentration of the latex to be a low value (VF=20%) and PS spheres could only cover about three fifths areas of the substrate, which would result in the self-assembly process in a quasi 2D plane.

Fig. 8 shows our simulation results when self-assembly temperature varies from 25℃ to 75℃. Fig. 8 (c) reveals that the the difference of the magnitudes of the first harmonics (M1) are not pronounced and we can find the largest power (17.72) is achieved at the temperature of 45 ℃, which indicates the line cracks and point defects of the crystal obtained at 45℃ are less than those obtained at other temperatures. We believe the little difference among M1 of different temperatures are the natural results of many empty areas in the simulation patterns caused by "low concentration latex" which are mixed with "defects". The difference among M2 and M3 are both more pronounced and they show the largest power, which correspond the best ordering, would be achieved at 45 ℃, indicating 45℃ is the optimized self-assembly temperature. Fig. 8 (a) and (b) are the Monte Carlo simulation Patterns and corresponding FT pattern, respectively. The bright and regular spots in the FT pattern reveal the good quality of the crystal shown in Fig. 8 (a). Our simulation data predict in gerneral that 45 ℃ is the optimized temperature for the PS spheres self-assembly.
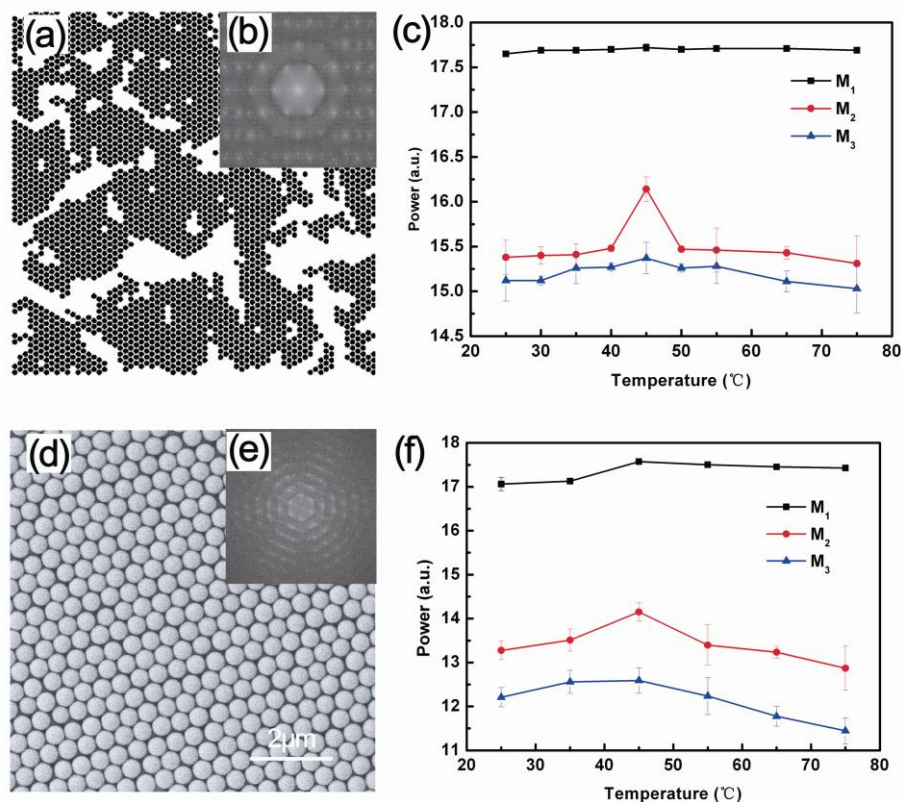

Fig. 8 The Monte Carlo simulation pattern of 45 ℃ (a) and corresponding typical scanning electron micrographs of the colloidal crystal treated at the temperature of 45 ℃ (d). Figure (b) and (e) show corresponding FT patterns of the panels (a) and (d). The panels (c) and (f) show magnitudes of the first three harmonics in the FT patterns obtained from the Monte Carlo simulations setting different temperature parameters and colloidal crystal treated at different temperatures, respectively. All the concentration of the latex are VF=20%.

The accuracy of our model may be tested by experimental

results. We implemented a series of PS self-assembly at different

temperatures, keeping other conditions constant: final spin-coating speed, VF of the latex and time were 3500 rpm, 20% and 30 seconds, respectively. The results are shown in Fig. 8 (d), (e) and (f). Fig. 8 (f) and Fig. 8 (c) show that the simulation results are well consistent with experiments: firstly, the first three harmonics variation trend in experiment is consistent with those in simulation; secondly, the best quality of colloidal crystal was indeed achieved at the temperature of 45 ℃. The second harmonins of the experiments (VF=20%) at 45 ℃ and 25℃ are 14.15 and 13.28, respectively, and we could expect more than 7% improvement of the sphere lattice ordering in the growth plane. Moreover, the ratio M_1/M_2 reduces from 1.3 in the sample obtained at 45 ℃ to 1.2 in the sample obtain at 25 ℃. This clearly corresponds to the improved sharpness and symmetry of lattice points in the SEM image of the sample using thermal treament. Consequently, defects are greatly reduced with the help of thermal treament.

What is more, the Monte Carlo simulation patterns and corresponding SEMs of the obtained colloidal crystal are also given in the supplementary information (Figure S5). It is very clear that the simulation patterns are similar to the experiments'. Both the experimental and simulation results are consistent with the following scenario: at the early stages, the initial nucleus was formed and then surrounding spheres transferred to the nucleus; eventually, large areas close-packed spheres arrays, namely colloidal crystal, were formed. Although we may achieve perfect crystal (without defects) theoretically, a few point and "line" defects (Figure S2 (b)) can still be found in the crystal obtained in optimized self-assembly condition, which is ascribed to the sensitivity of the quality of the crystal to the complex self-assembly condition, such as concentration of the latex and the wetting of the substrates, etc. However, the method we proposed have greatly improved both the scale and the quality of the resultant colloidal crystal.

4. Conclusions

We have demonstrated the formation of high-quality, wafer-scale, two dimensional colloidal crystals using the new method, namely thermally assisted self-assembly of polystyrene spheres. Moreover, we improved the traditional self-assembly theory and simulated the self-assembly process using modified Monte Carlo method. The model can predict the optimized self-assembly temperature. And the method is not only less time-consuming but also easier to control. We believe our method can also be applied to self-assembly of PS spheres with other diameters. What's more, this approach is highly compatible with contemporary microfabrication which may accomplish the eventual mass production of low-cost practical devices, including nano-lithography, photonics, data storage, biosensors, and plasmonics, etc.

Acknowledgements

Notes and references

a USTC....

† Electronic Supplementary Information (ESI) available. See DOI: 10.1039/b000000x/
‡ Footnotes should appear here. These might include comments relevant to but not central to the matter under discussion, limited experimental and spectral data, and crystallographic data.

1. J. H. Zhang, Y. F. Li, X. M. Zhang and B. Yang, *Adv. Mater.*, 2010, **22**, 4249-4269.
2. G. Ctistis, P. Patoka, X. Wang, K. Kempa and M. Giersig, *Nano Letters*, 2007, **7**, 2926-2930.
3. H. Xu and W. A. Goedel, *Small*, 2005, **1**, 808-812.
4. S. D. Jiang, J. Ichihashi, H. Monobe, M. Fujihira and M. Ohtsu, *Optics Communications*, 1994, **106**, 173-177.
5. F. Marlow, Muldarisnur, P. Sharifi, R. Brinkmann and C. Mendive, *Angewandte Chemie-International Edition*, 2009, **48**, 6212-6233.
6. J. F. Galisteo-Lopez, M. Ibisate, R. Sapienza, L. S. Froufe-Perez, A. Blanco and C. Lopez, *Adv. Mater.*, 2011, **23**, 30-69.
7. E. Betzig, J. K. Trautman, R. Wolfe, E. M. Gyorgy, P. L. Finn, M. H. Kryder and C. H. Chang, *Applied Physics Letters*, 1992, **61**, 142-144.
8. S. H. Sun, C. B. Murray, D. Weller, L. Folks and A. Moser, *Science*, 2000, **287**, 1989-1992.
9. M. M. Baksh, M. Jaros and J. T. Groves, *Nature*, 2004, **427**, 139-141.
10. A. J. Haes, S. L. Zou, G. C. Schatz and R. P. Van Duyne, *J. Phys. Chem. B*, 2004, **108**, 109-116.
11. M. Retsch, M. Tamm, N. Bocchio, N. Horn, R. Forch, U. Jonas and M. Kreiter, *Small*, 2009, **5**, 2105-2110.
12. N. Vogel, M. Jung, N. L. Bocchio, M. Retsch, M. Kreiter and I. Koper, *Small*, 2010, **6**, 104-109.
13. N. Vogel, C. K. Weiss and K. Landfester, *Soft Matter*, 2012, **8**, 4044-4061.
14. N. D. Denkov, O. D. Velev, P. A. Kralchevsky, I. B. Ivanov, H. Yoshimura and K. Nagayama, *Nature*, 1993, **361**, 26-26.
15. T. P. Bigioni, X. M. Lin, T. T. Nguyen, E. I. Corwin, T. A. Witten and H. M. Jaeger, *Nature Materials*, 2006, **5**, 265-270.
16. R. D. Deegan, O. Bakajin, T. F. Dupont, G. Huber, S. R. Nagel and T. A. Witten, *Nature*, 1997, **389**, 827-829.
17. P. Jiang and M. McFarland, *J. Am. Chem. Soc*, 2004, **126**, 13778-13786.
18. P. J. Yunker, T. Still, M. A. Lohr and A. G. Yodh, *Nature*, 2011, **476**, 308-311.
19. W. Khunsin, G. Kocher, S. G. Romanov and C. M. S. Torres, *Adv. Funct. Mater.*, 2008, **18**, 2471-2479.
20. H. W. Deckman and J. H. Dunsmuir, *Applied Physics Letters*, 1982, **41**, 377-379.
21. C. Dux and H. Versmold, *Physical Review Letters*, 1997, **78**, 1811-1814.
22. U. C. Fischer and H. P. Zingsheim, *Journal of Vacuum Science & Technology*, 1981, **19**, 881-885.
23. A. T. Skjeltorp and P. Meakin, *Nature*, 1988, **335**, 424-426.
24. P. A. Kralchevsky and K. Nagayama, *Advances in Colloid and Interface Science*, 2000, **85**, 145-192.
25. K. Skidmore, *Semiconductor International/Semiconductor International*, 1987, **10**, 80-85.
26. J. H. Zhang, Z. Chen, Z. L. Wang, W. Y. Zhang and N. B. Ming, *Materials Letters*, 2003, **57**, 4466-4470.
27. W. Khunsin, A. Amann, G. Kocher-Oberlehner, S. G. Romanov, S. Pullteap, H. C. Seat, E. P. O'Reilly, R. Zentel and C. M. S. Torres, *Adv. Funct. Mater.*, 2012, **22**, 1812-1821.
28. S. Middleman, *Journal of Applied Physics*, 1987, **62**, 2530-2532.
29. R. Mayoral, J. Requena, J. S. Moya, C. Lopez, A. Cintas, H. Miguez, F. Meseguer, L. Vazquez, M. Holgado and A. Blanco, *Adv. Mater.*, 1997, **9**, 257-&.
30. P. A. Kralchevsky and K. Nagayama, *Langmuir*, 1994, **10**, 23-36.
31. S. M. Woodley and R. Catlow, *Nature Materials*, 2008, **7**, 937-946.
32. D. J. Wales and H. A. Scheraga, *Science*, 1999, **285**, 1368-1372.
33. L. Filion, M. Marechal, B. van Oorschot, D. Pelt, F. Smallenburg and M. Dijkstra, *Physical Review Letters*, 2009, **103**.